ICSV14
Cairns • Australia
9-12 July, 2007

14th International Congress on Sound & Vibration

AEROACOUSTIC COMPUTATIONS OF A COUNTER-ROTATING FAN

Cyril Polacsek, Raphael Barrier

Office National d'Etudes et de Recherches Aérospatiales
Departments of Numerical Simulations & Aeroacoustics and Applied Aerodynamics
29, avenue de la Division Leclerc
92322 Châtillon Cedex, France
cyril.polacsek@onera.fr

Abstract

Aeroacoustic simulation of interaction noise generated by a contrafan model is proposed in this paper, in the framework of European Project VITAL (EnVIronmenTALly friendly aeroengine). Main objective here is to check the ability of advanced computations, including noise generation, propagation and radiation, to give a reliable evaluation of an innovative concept. Numerical simulations are realized by using a hybrid method based on the coupling of CFD (Computational Fluid Dynamics) and CAA (Computational Aero-Acoustics) ONERA codes. The matching between CFD and CAA is based on a Fourier-Bessel mode expansion of the perturbation field along a prescribed cross-section, from which outgoing modes then are traduced, in an original way, as source terms in the CAA. In-duct mode power and spectrum at the outer-wall are analyzed and discussed by comparison with theory and with similar results from project partners. Acoustic far field radiated by inlet and deduced from Kirchhoff integration is addressed in terms of mode spectrum and directivities. These first predictions are to be compared to experimental data soon available.

1. INTRODUCTION

Fan noise generated by rotor-stator interaction mechanisms is the major tone source component of high-bypass ratio aeroengines during take-off and approach conditions. A great attention is paid nowadays to try to reduce these discrete frequency tones highly contributing to the OASPL (Overall Sound Pressure Level), especially as air traffic is growing and environmental rules become drastic. An alternative to more conventional approaches for producing next generation of low-emission and low-noise aircraft engines is to investigate new architectures like the counter-rotating fan. Aeroacoustics of a contrafan model is studied in this paper, in the framework of European Project VITAL (EnVIronmenTALly friendly aeroengine).
The CRTF (Counter-Rotating TurboFan) 1/4 scale model studied here consists in a 560 mm diameter fan made of a 10-bladed upstream rotor and 14-bladed downstream rotor. Tests are planned at the Russian CIAM (Central Institute of Aviation Motors) rig facility [1]. Flight

configuration considered is the certification point at approach conditions. Following the same way as many authors from the aeroacoustic community [2-4], numerical simulations are realized by using a hybrid method based on the coupling of CFD (Computational Fluid Dynamics) and CAA (Computational Aero-Acoustics) ONERA codes [5]. CFD is performed using a RANS solver from *elsA* platform [6,7], providing both mean flow and perturbation field required for acoustics. Industrial complex configurations like the contrafan can be practically achieved using an implemented chorochronicity technique [8], which permits the computation of the stage aerodynamics over a single rotor1-rotor2 passage. CAA is performed using the time-domain Euler solver from *sAbrinA* platform [9, 10]. The matching between CFD and CAA is based on a Fourier-Bessel mode expansion [11] of the perturbation field along a prescribed cross-section, assuming annular geometry and uniform mean flow at the interface. Outgoing cut-on modes then are re-generated in an original way [12] by means of equivalent monopoles that are entered as source terms in *sAbrinA*. The matching procedure is achieved using ONERA code *ExFan*. Finally, acoustic near field is extrapolated to the far field by using of a Kirchhoff integral.

Firstly, the paper gives a short description of the contrafan model and points out essential theoretical results proposed by Hanson [13] from counter-rotating propeller and fan studies. Interaction mode description is mandatory for preparing the computations and for checking the numerical results. Then the paper presents the numerical tools. The CFD part focuses on the phase-lagged approach, computation domain and grid definition. After a brief overview of the mode matching approach (already detailed in [5,12]), the paper is devoted to the propagation of interaction modes with *sAbrinA*. The computation domain, the grid definition, and the coupling with Kirchhoff are outlined. Last section of the paper is devoted to the aeroacoustic analyzes. Unsteady aerodynamics post-processed results related to the acoustics are presented and discussed. In-duct mode spectrum power is also discussed by comparing the results obtained from VITAL partners involved in this task. Finally, acoustic far field deduced from kirchhoff integration is addressed in terms of mode spectrum and OASPL directivities.

2. COUNTER-ROTATING FAN DESCRIPTION

The CRTF model is 560 mm diameter and is equipped with a 10-bladed upstream rotor1 ($B_1 = 10$) and a 14-bladed downstream rotor2 ($B_2 = 14$). The studied case is a certification point at approach condition for which rotation frequencies respectively are equal to 4633.3 and 4169.3 rpm (speed ratio equal to 0.9), giving in hertz, $N_1 = 77.2$ Hz and $N_2 = 69.5$ Hz. Thermodynamic conditions are imposed by a mass flow rate of 24.4 kg.sec^{-1}. The fan will be mounted in the CIAM C3-A test-rig. A 3D skin mesh view of the contrafan provided by SNECMA is shown in Fig. 1, and a basic sketch of the aerodynamic vein is also given in Fig. 2. Modal analyzes can be assessed using a microphone ring at the outer wall, visible in Fig. 2. The hub-to-tip ratio, h, is close to 0.3 in the rotor1 plane with an axial mean Mach number roughly equal to $M = 0.25$ near the hub nozzle. In this paper we are focusing on the upstream propagation and radiation by the inlet. In-duct and far-field measurements should be soon available (tests have been delayed) to make comparisons with the numerical predictions.

3. INTERACTION FREQUENCY-MODES

Analytical formulations proposed by Hanson [13] generalize the well-known Tyler and Sofrin theory limited to a single rotor (standard rotor-stator case). Interaction frequencies, f_{12}, and respective spinning modes, m, are addressed by the following expressions:

$$f_{12} = \left| n_1 B_1 N_1 + n_2 B_2 N_2 \right| , \qquad m = n_1 B_1 - n_2 B_2$$

In these equations, n_1 and n_2 are positive or negative integers, and the sign of the spinning mode m is defined with respect to the rotor1. Usual expressions for rotor-OGV case are retrieved by setting $N_2 = 0$ and $B_2 = V$. Note that contrarily to rotor-stator configurations, the interaction tones are not harmonics of rotor1 nor rotor2, since angular modes obtained for $n_1 = 0$ or $n_2 = 0$ are practically cut-off in ducted fans. The determination of theoretical axial wavelength, $\lambda_{m\mu}$, relative to the interaction mode (m,μ) is then used to adjust the grid spacing of the CFD and CAA grids, as discussed in section 4. The five first interaction tones with associated cut-on modes obtained in the inlet region just behind the hub nozzle ($h = 0$ and $M = 0.23$) are summarized in the table below. The axial wavelength λ_{m1} indicated in the table is the smallest one with respect to the angular mode m.

Table 1. Interaction tone characteristics in the inlet region

Frequency f_{12}	$B_1N_1+B_2N_2$ (1745 Hz)	$2B_1N_1+B_2N_2$ (2517 Hz)	$2B_1N_1+2B_2N_2$ (3490 Hz)	$3B_1N_1+2B_2N_2$ (4262 Hz)	$3B_1N_1+3B_2N_2$ (5235 Hz)
Angular cut-on modes	***-4***	***6***	***-8***	***2***	***-12***
Radial cut-on modes	***1,2***	***1-3***	***1-3***	***1-6***	***1-4***
λ_{m1} *(m)*	***0.174***	***0.12***	***0.084***	***0.061***	***0.056***

4. COMPUTATION METHODS

4.1 RANS calculations

CFD computations are performed using the 3D Navier-Stokes code *elsA* that solves the compressible RANS equations in the relative frame with a cell-centered finite volume formulation. Space discretization is ensured using Jameson's second-order-centered scheme with the addition of an artificial viscosity. Stagnation pressure and enthalpy are assigned at the inlet plane and radial equilibrium of static pressure is imposed at the two exit planes. Wall boundary conditions are applied to blades, casing and hub. Turbulence closure is achieved using the k-l turbulence model of Smith [14]. Unsteady computations are performed using a phase-lagged approach [8] assuming classically that the unsteady effects are only due to the rotation and that the flow is periodic in the frame of reference of the blade rows. The CFD multi-block grid, presented in Fig.3, uses a total number of 4,900,000 points. The splitter downstream the second rotor has been taken into account due to its vicinity of the blade rows. Steady RANS mean flow solution required for CAA is achieved by performing a 2D-axi computation taking into account the real inlet geometry (Fig. 3, right). However, in order to ensure the convergence of the 3D steady and unsteady RANS computations, the CFD domain is extended upstream and downstream as an infinite annular (cylindrical upstream) duct, without altering the mean flow and perturbation field near the source region (matching region). Thus, the mesh can be easily stretched up at both the inlet and exit planes (see Fig. 3, left), which permits to increase the numerical dissipation and to reduce acoustic wave reflections. As visible on the figure too, the mesh density is highly increased between the two rotors to capture with accuracy the first rotor wake and its interaction with the second rotor. According to the parametric studies achieved in TurboNoiseCFD European Project, a minimum resolution of 40 points per acoustic wavelength (see Table 1) is imposed in the region upstream of the fan to correctly propagate the acoustic modes.

4.2 Euler/Kirchhoff calculations

Acoustic propagation is simulated using the 3D structured multi-block CFD/CAA platform, *sAbrinA*, developed at ONERA. Details about the solver can be found in Refs [9,10]. *sAbrinA* uses a low dispersive 6th-order scheme in space and a 3rd-order Runge-Kutta scheme for the time integration. RANS mean flow computed by *elsA* has to be interpolated from the CFD to the CAA grid, which is performed using Tecplot. Euler calculation is coupled to a Kirchhoff integral used to extrapolate the solution up to the far field. Because interaction noise simulations are practically limited to first dominant tones (generated by means of harmonic sources in the code), the Kirchhoff formulation is written in the frequency domain for convenience as explained in [5]. Conventional Thomson approach enhanced by a grid stretching near the external boundaries is used in the present study to simulate free-space conditions. Non-dispersive and non-dissipative acoustic propagation is ensured using $\lambda/10$ grid spacing in the axial direction, λ denoting the smallest axial wavelength to be considered, and directly related to the values in Table 1. 3D and section views of the grid are shown respectively in Fig. 4 and 5. As seen in the figure 5, in order to limit the grid size (about 500,000 points), the mesh cells are stretched rapidly outside of the duct, as the acoustic wavelengths are expected to become naturally higher. The time spacing is adjusted so that the CFL number is almost equal to 1, in order to limit the number of time iterations. CPU time required to get a fully converged solution is about 13 hours (39,000 iterations) on a NEC SX5.

4.3 Mode matching

The propagation model proposed to match RANS and Euler calculation is the solution of the convected-wave equation in an annular duct. Rienstra proposes a more general multiple-scale solution taking into account for a slowly varying duct section [11], but we limit here to the conventional uniform-flow/annular-duct assumption for having a simple mathematical expression of the Green's function, in order to get back easily to the sources. The complex amplitudes of expanded modes can be obtained by using a Fourier-Bessel transform of pressure disturbance field in a single cross section. A wave-splitting technique [15] is applied to identify the mode direction and then to retrieve the outgoing modes to be considered (incoming wave contribution being removed). The key point of our matching approach is that the expanded modes are entered as equivalent sources in the CAA, whereas they are generally traduced (directly) in terms of a boundary condition. The inverse-like procedure to get back to the sources (complex amplitude) is detailed in [5,12]. Here, the source term is constructed by summing over all interaction tones, f_{12}, and over all associated propagating modes (m,μ), including practically the first cut-off radial modes. Expanded modes and equivalent sources both are computed using ONERA Matlab code *ExFan*.

5. AEROACOUSTIC ANALYZES

5.1 Unsteady aerodynamic post-processed results

The unsteady computation starts from a converged steady state solution and takes about 2 relative revolutions to achieve a converged unsteady prediction. Convergence is achieved when the mass flow history in several axial sections shows a repeatable oscillation cycle around the target value (24.4 kg.sec^{-1}). Once the computation is converged, the CFD/CAA coupling method requires to build a periodic solution in the absolute frame. Using periodicity

relations at chorochronic boundaries (rotor1-rotor2 passage), a continuous reconstructed solution over a full revolution in the absolute frame can be obtained, as observed on the entropy snapshot plotted in Fig. 6. The phase-lagged reconstruction then is performed in the CFD/CAA matching section to provide the perturbation field required for acoustics. A snapshot of the static pressure in this section is shown Fig. 7.
The frequency-mode spectrum (outgoing waves) obtained by the matching processing (using *ExFan*) is presented in Fig. 8, in which the five interaction tones with respective angular mode order are clearly addressed, in agreement with the theory (section 3). The intensity of second interaction tone (f_{12} = 2517 Hz, m = 6) appears to be dominant. This estimated balance of outgoing mode levels of course is determinant for the prediction of radiated noise. While waiting to have experimental data (modal analyzes), these predictions were compared with those obtained by other VITAL partners also involved in aeroacoustic simulations (using their own methods). Figure 9 shows a comparison of inlet duct acoustic power (dB) computed by ONERA (in blue), CIAM (in red), and DLR (in green). The power levels of the five first interaction tones are roughly balanced in the same way, which gives some confidence in the simulations. However, large differences in the levels (relative to the same tone) can be noticed, particularly on the third interaction tone (f_{12}= 3490 Hz). These predictions have to be related to the experiment if one wants to go further in the discussion.

5.2 CAA results: inlet propagation and far-field radiation

Although all tones can be generated at the same time in sAbrinA, first computations were run on the first tone only, in order to carefully check the simulations. Thus, a snapshot of acoustic propagation of single mode (-4,1) on first interaction tone (1745 Hz) is visualized in Fig. 10. Sources are injected in the matching plane (x = -0.4 m), and waves are able to propagate in the upstream and downstream direction, in a realistic mean flow provided by the steady RANS solution. The iso-contour plots show a clean representative mode pattern with expected upstream/downstream convection effects, and thanks to the stretching, acoustic waves are numerically “absorbed” as they reach the inlet and outlet boundaries of the CAA grid. Next basic analysis was devoted to the generation of all radial modes (two cut-on, μ = 1-2, and first cut-off, μ = 3) on same interaction tone (1745 Hz). Figure 11 shows RMS pressure field computed by sAbrinA by coupling the CAA output with a Kirchhoff integral. The coupling with Kirchhoff permits to extend the CAA near-fied solution up to the far field without introduce any visible discontinuity across the Kirchhoff surface (indicated in the figure), and provides a clean directivity pattern. The same analyzes then are made when the five tones with associated angular and radial modes are generated all at once, as shown in Fig. 12. The sound pressure fields here are expressed in dB (OASPL). Here again, the coupling with Kirchhoff allows us to extend the predictions up to the far field, revealing a high directional directivity pattern. Finally, far-field noise at location of microphone antenna (to be used in the C3-A rig) is calculated for each tone (SPL) and for all 1-5 tones (OASPL). Results are summarized in Fig. 13, showing that the overall level is mainly due to the second tone, other tones only contributing to the OASPL near the axis direction (0°). First and second interaction tones are highly directional and are determining the directivity shape with a maximum lobe around 35 degrees.

6. CONCLUSIONS

A hybrid method based on the coupling of CFD (RANS) and CAA (Euler) ONERA codes has been presented and applied to provide aeroacoustic characteristics of a counter-rotating fan model. Source generation is expected to be caused by interaction mechanism and are ideally

related to the usual interaction mode theory extended to fully rotating rows. Outgoing modes deduced from unsteady RANS solution were found to be in agreement with interaction modes expected from theory. In-duct power levels predicted by different numerical methods (and different codes) proposed by VITAL partners have shown similar trends with respect to SPL tone balance over the spectrum. However, these first comparisons have revealed high discrepancies in the SPL of each respective tone, so that acoustic measurements are required to go further in the discussion. These differences are not really surprising when considering the difficulty for the CFD to simulate with accuracy noise source generated by a contrafan. Anyway, present hybrid method appears to be reliable, showing its ability to include the dominant interaction tones (up to 5 kHz), which was a challenging case for numerical simulations. Predicted OASPL directivities show that the radiated noise level is mainly due to second interaction tone (2517 Hz) and characterized by a high directional pattern focalized around 30-40 degrees.
Next step of course will be to relate these predictions to the measurements (tests should start in May 2007), and also to compare the counter-rotating fan aeroacoustics with a standard architecture like SNECMA CFM56 engine. These activities are planned in the framework of VITAL project (2006-2008).

REFERENCES

[1] I.A. Brailko, V.I. Mileshin, M.A. Nyukhitov, S.V. Pankov, "*Computational and Experimental Investigation of Unsteady and Acoustic Characteristics of Counter-Rotating Fans*", ASME HF-FED-2004-56435, Charlotte (USA), 2004.

[2] V. Ahuja, Y. Ozyoruk, L. N. Long, "*Computational simulations of fore and aft radiation from ducted fans*", AIAA 2000-1943, 6th AIAA/CEAS, Lahaina (Hawaii), 2000.

[3] R. T. Biedron, C. Rumsey, G. G. Podboy, M. H. Dunn, "*Predicting the Rotor-Stator Interaction Acoustics of a Ducted Fan Engine*", 39th AIAA ASME, Reno (USA), 2001.

[4] X. Zhang, X. X. Chen, C. L. Morfey, and B. J. Tester, "*Computation of Fan Noise Radiation through a Realistic Engine Exhaust Geometry with Flow*", AIAA 2003-3267, 9th AIAA/CEAS, Hilton Head (USA), 2003.

[5] C. Polacsek, S. Burguburu, S. Redonnet, M. Terracol, *Numerical Simulations of Fan Interaction Noise Using a Hybrid Approach*, AIAA Journal, Vol. 44, No. 6, 2006.

[6] G. Billonnet, A. Fourmaux, C. Toussaint, "*Evaluation of two competitive approaches for simulating the time-periodic flow in an axial turbine stage*", 4th European Conference on Turbomachinery, Firenze (Italy), 2001.

[7] L. Cambier, M. Gazaix, "*elsA: An Efficient Object-Oriented Solution to CFD Complexity*", 40th AIAA Aerospace Sciences Meeting and Exhibit, Reno (USA), 2002.

[8] A. Fourmaux, "*Assessment of a low storage technique for multi-stage turbomachinery Navier-Stokes computation*", ASME Winter annual meeting, Chicago (USA), 1994.

[9] M. Terracol, E. Labourasse, E. Manoha, P. Sagaut, "*Numerical Simulation of the 3D Unsteady Flow in a Slat Cove for Noise Prediction*", AIAA-2003-3110, 9th AIAA/CEAS, Hilton Head (USA), 2003.

[10] S. Redonnet, E. Manoha, and O. Kenning, "*Numerical Simulation of the Downstream Fan Noise and Jet Noise of a Coaxial Jet with a Shielding Surface*", 10th AIAA/CEAS, Manchester (UK), 2004.

[11] N. C. Ovenden, S. W. Rienstra, *Mode-matching Strategies in Slowly Varying Engine Ducts*, AIAA 2003-3139, 9th AIAA/CEAS, Hilton Head (USA), 2003.

[12] C. Polacsek, "*An equivalent source model for simulating turbofan interaction noise*", Internoise Conference, Honolulu (Hawaï), 2006

[13] D.B. Hanson, "*Noise of counter-rotation propellers*", AIAA Paper 84-2305 & Journal of Aircraft, Vol. 22, no. 7, 1985.

[14] B.R. Smith, "*The k-l turbulence model and wall layer model for compressible flows*", AIAA Paper 90-83, 21st Fluid and Plasma Dynamics Conference, Seattle (USA), 1990.

[15] R. P. Dougherty, *A wave-splitting technique for nacelle acoustic propagation*, AIAA Paper 97-1652, 3rd AIAA/CEAS Aeroacoustics Conference, Atlanta (USA), 1997.

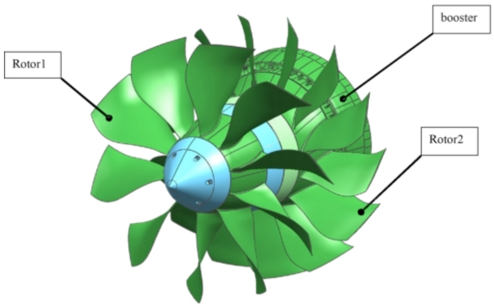

Fig. 1 Contrafan model (SNECMA)

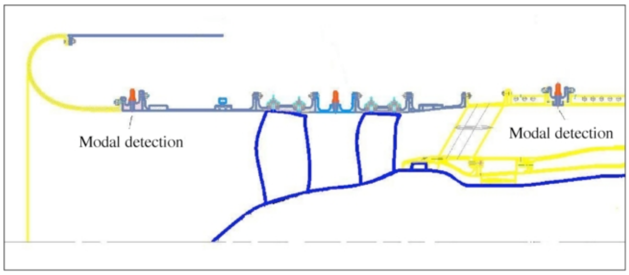

Fig. 2 Sketch of the aerodynamic vein in C3-A rig

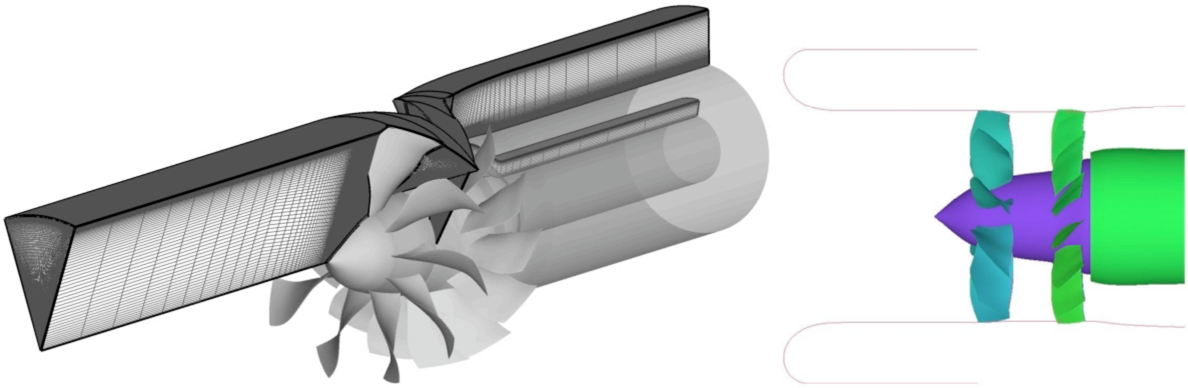

Fig. 3 CFD multi-block grid (left); hub and row color mesh skin with inlet duct boundary (right)

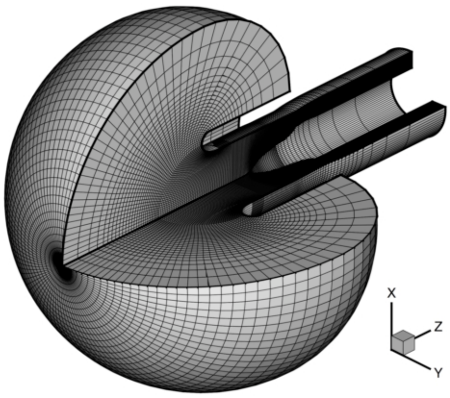

Fig. 4 3D view of CAA grid

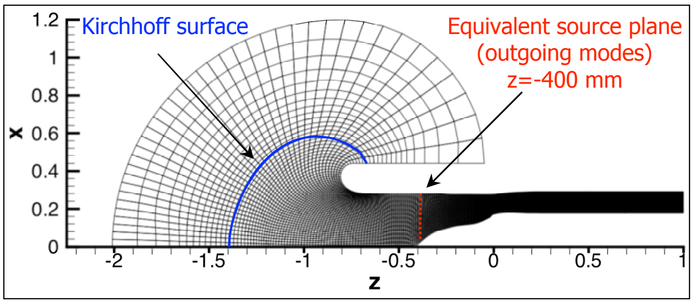

Fig. 5 Section view with Kirchhoff surface and eq. sources location

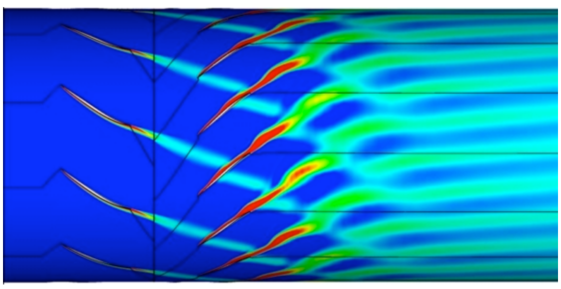

Fig. 6 Reconstructed entropy snapshot at 60% span

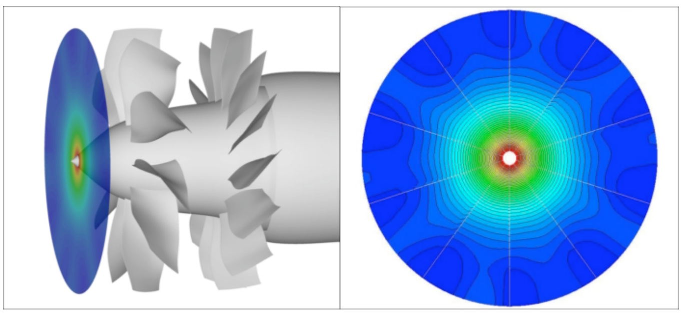

Fig. 7 Instantaneous static pressure in the matching section

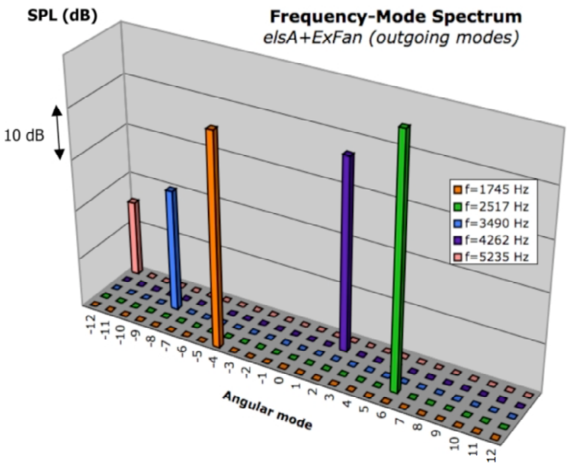

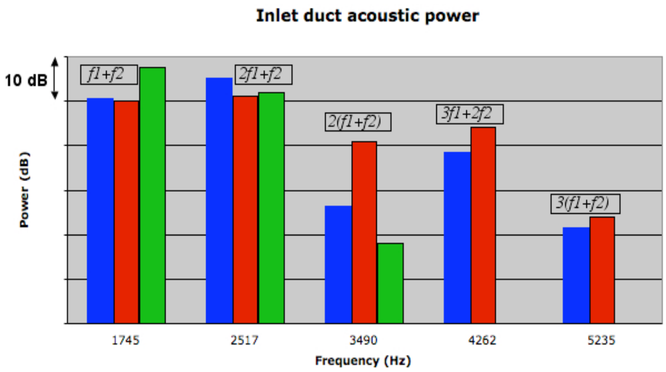

Fig. 8 Interaction mode spectrum (outgoing wave) deduced from RANS using ExFan routine

Fig. 9 Comparison of acoustic power predictions from VITAL partners: ONERA (blue), CIAM (red), DLR (green)

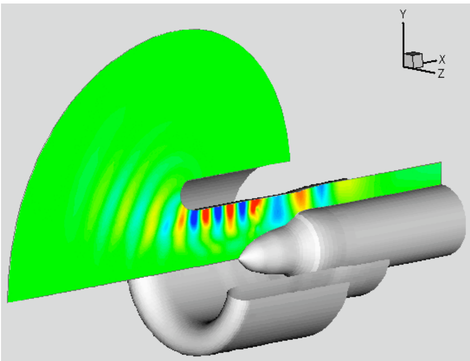

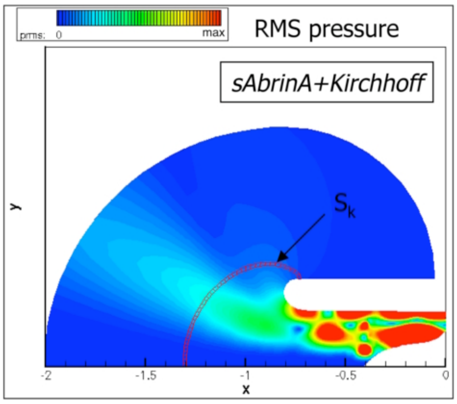

Fig. 10 Single mode propagation using sAbrinA: mode (4,1) ; f_{12} = 1745 Hz

Fig. 11 RMS pressure field on first tone using sAbrinA coupled with Kirchhoff

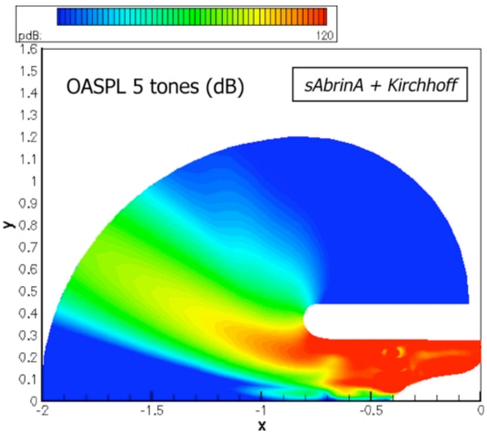

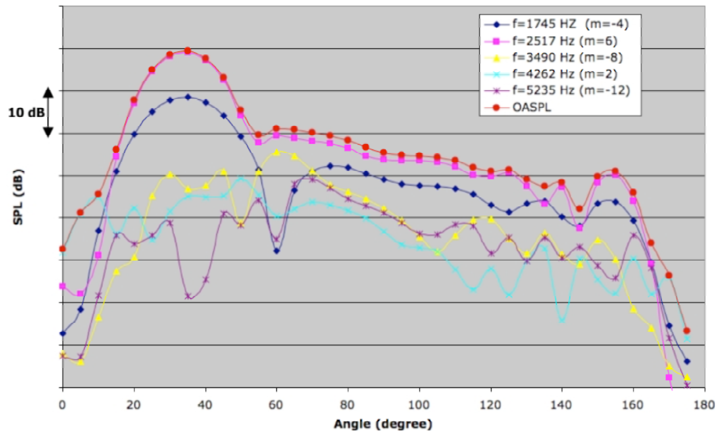

Fig. 12 OASPL pressure field on all (1-5) tones

Fig. 13 SPL (single tone) and OASPL (5 tones) predicted far-field directivities